J Mater Sci (2010) 45:6325–6331
DOI 10.1007/s10853-010-4452-1

IMEC 2009

Thin film deposition using a plasma source with a hot refractory anode vacuum arc

Isak I. Beilis · Yosef Koulik · Raymond L. Boxman · David Arbilly

Received: 29 December 2009 / Accepted: 27 March 2010 / Published online: 8 April 2010

Abstract Vacuum arc generated plasma was used to deposit metallic Al, Zn, and Sn coatings on glass substrates. An arc mode with a refractory anode and an expendable cathode (the "hot refractory anode vacuum arc"), overcomes macroparticle (MP) contamination experienced in other arc modes. $I = 100$–225 A arcs were sustained between a water-cooled coating source cathode and an anode, which was heated by the arc, separated from each other by a 10-mm gap, for times up to 150 s. The distance from the arc axis to the substrate (L) was 80–165 mm. Film thickness was measured with a profilometer. It was found that the deposition rate increased with time to a peak, and then decreased to a steady-state value. The peak occurred earlier when using short anode (9 mm long), e.g., with the Al cathode, $L = 110$ mm, and $I = 200$ A, the peak was at $t_p = 15$ s after arc ignition while with the long anode $t_p = 45$ s. t_p decreased with I, from 45 s with $I = 100$ A, to 10 s with $I = 225$ A with the short anode. The peak is believed to appear due to initial condensation of cathode material (including MPs) on the cold anode, and its subsequent evaporation as the anode heated. In the later HRAVA steady state, a balance between condensation and evaporation on the anode is established. The deposition rate peak was significant with low melting temperature Al and Zn cathodes, which produce many MPs, and negligible with Cu and Ti cathodes.

I. I. Beilis (✉) · Y. Koulik · R. L. Boxman · D. Arbilly
Electrical Discharge and Plasma Laboratory, School of Electrical Engineering, Tel Aviv University, P.O. Box 39040, Tel Aviv 69978, Israel
e-mail: beilis@eng.tau.ac.il

Introduction

Metallic plasma sources are applied in material processing for highly energetic ion implantation, thin film and coating deposition, nanostructure formation, and integrated circuit manufacturing [1]. Different techniques was used for thin film deposition (including Al and Zn), the physical vapor deposition (PVD) such as evaporation source [2, 3], magnetron sputtering [4–6], the pulse laser deposition [7], and the electroplating [8]. Vacuum arc deposition (VAD) is one of PVD techniques that was intensively studied in the last decades [9], largely with the goal of obtaining clean plasma, without macroparticle (MP) contamination. Various types of vacuum arcs are currently used for VAD. In the "cathodic" arc, the plasma generated in a small region of a consumable cathode known as the cathode spot [10], and is then transported to a substrate upon which it condenses to form a thin film or coating. MP-free thin metallic film coatings can be deposited using cathodic vacuum arc with MP filtering [11]. In the hot electrode vacuum arc, either anode [12] or cathode material [13] is evaporated from a broad area of the surface of a consumable anode or cathode, and then transported to the substrate.

A plasma source for metallic deposition with strongly reduced MP contamination using a hot refractory anode vacuum arc (HRAVA) was investigated [14]. HRAVA processing was reviewed recently [15]. The HRAVA is sustained between a cooled cathode and a thermally isolated anode (Mo, W, C) and usually started as a cathodic arc. Initially, the anode is cold and the vapor and plasma generation are localized at cathode spots. The anode is heated by the arc until sufficiently hot so that metal vapor (and MPs) originating at the cathode and condensed on the anode previously, is re-evaporated from the hot anode. The generated anodic metallic plasma expands radially from the

interelectrode gap. Relatively high deposition rates (e.g., up to ~3.6 μm/min with a Cu cathode arc current $I = 300$ A), dense plasma in the gap ($\geq 10^{14}$ cm^{-3}) [16] and high anode temperatures (e.g., 2500 K on W anodes) were obtained [15].

The HRAVA deposition characteristics were investigated for Cu, Ti, Cr cathodes [14, 15, 17]. However, HRAVA with cathodes have low melting temperature (e.g., Zn and Sn) were not considered previously. These materials are important for depositing optical films from their oxides. The main goal of this paper is to present the results of an experimental study of the HRAVA deposition characteristics with Al, Zn, and Sn cathodes.

Experimental setup and methodology

Experimental apparatus and electrodes assembly

Experiments were conducted in a cylindrical vacuum chamber (400 mm length, 160 mm diameter), as shown schematically in Fig. 1. The chamber was pumped by a diffusion pump to 1.3×10^{-2} Pa. During the arc, the pressure in the chamber was 5.3×10^{-2} Pa. The arc was sustained between a water-cooled Al, Zn, and Sn source cathodes and refractory (graphite, Mo, and W) anodes, for times up to 150 s, and current (I) of 100–225 A. Cathode and anode material and geometry are presented in Table 1.

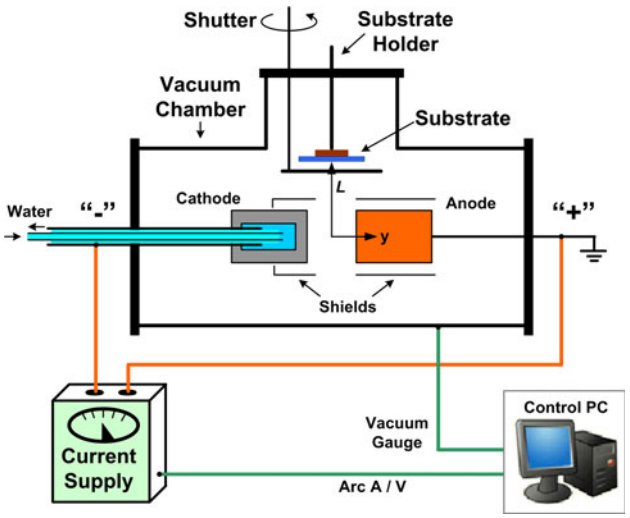

Fig. 1 Schematic diagram of the chamber and cathode–anode assembly

A stainless steel cylindrical radiation shield of 70 mm diameter surrounded the anode to reduce radiative heat losses during Al and Zn deposition. The anode was supported by a thin tungsten rod that also connected it to the electrical circuit. The cathode was surrounded by a boron nitride square box shaped shield with side 65 mm and positioned at different axial locations relative to the cathode surface. The shield blocked MP flux originating at cathode spots on the side of the cathode from reaching the substrate, and to prevent MP flux originating on the cathode face from reaching a portion of the substrate. The W anode used with Sn cathode was relatively thin, and the radiation shield was not required; also no shield was placed around the Sn-filled Cu cup. The inter-electrode gap was about 1 cm.

Substrate preparation and mounting

The substrates were 76 × 26 mm^2 glass microscope slides. The substrates were pre-cleaned by liquid soap and water, and were then soaked in alcohol. The substrate mounted on a holder which was movable in the radial direction, were positioned at distances of 80–165 mm from the electrode axis, facing the plasma flux emanating from the inter-electrode gap. The holder was separated from the arc chamber by a shutter (Fig. 1) which controlled the deposition onset and exposure duration (15 s).

Coating characterization

As it was established previously in refs [14, 15, 17], the HRAVA coating was characterized by two different regions (see also below): A-region (practically without MPs) and C-regions (with MPs contamination similar to the coating by conventional arc jet). The MP and the deposited films were characterized in the A-region (about 3–5 mm from the boundary of A–C regions). The MP number was counted with an optical microscope and digital camera, which could detect MPs larger than approximately 1 μm. The MP density was defined by counting the total MP number per mm square, as described previously [18].

Table 1 Cathode and anode material and geometry

Cathode			Anode		
Material	Length, mm	Diameter, mm	Material	Length, mm	Diameter, mm
Al	40	30	Graphite	30	32
				9	32
Zn	25	30	Mo	30	32
Sn	10	60 (in Cu cup)	W	10	60

The film thickness was measured by profilometry after various arc durations beginning from arc ignition when the shutter was open for a pre-determined exposure time. The deposition rate (V_{dep}) was determined as the ratio between the incremental film thickness growth during the exposure time divided by this deposition times.

Experimental results

Arc visualization

Photographs of 175 A arcs with Al, Zn, and Sn cathodes (without shields) 30 s after arc ignition are shown in Fig. 2. The Al arc emission color is light green while the Zn is blue and Sn is green color. Cathode spot appeared on the cathode surface while the anodes were covered by a diffuse discharge. Later ($t > 30$–60 s) an anodic plasma plume filled most of the electrode gap and expanded in the radial direction.

Film morphology

Two characteristic regions with sharply different MP densities were observed on the substrate surface, as observed previously after Cu deposition [14, 17, 18]. Typical micrographs of Al films from the two regions are shown in Fig. 3: (1) the "A-region" facing the anode with few MPs (Fig. 3a) and (2) the "C-region" facing the cathode with many MPs (Fig. 3b).

Deposition rate

Aluminum

Figure 4 presents the measured Al deposition rate dependence on time from arc ignition, with I as a parameter, using a 30-mm long graphite anode, and the cathode recessed 3 mm inside into the square box shaped shield. It can be seen that V_{dep} increased with time to a peak, and then decreased to a steady-state value. The peak value ($\sim$0.7–0.8 μm/min) weakly depended on the current and the peak time decreased with I. The maximal deposition rate increased with arc current when the cathode surface was flush mounted or protruded 3 mm above the end of the shield. The dependence of maximal deposition rate on the cathode position with respect to the cathode shield is demonstrated in Fig. 5. The rate was $V_{dep} \sim 1.2$ μm/min when cathode surface was flush mounted with the shield

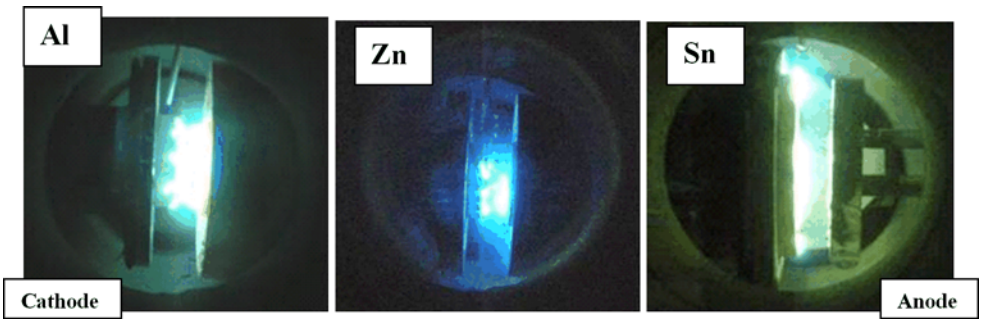

Fig. 2 Arc photographs with Al and Zn and Sn cathodes

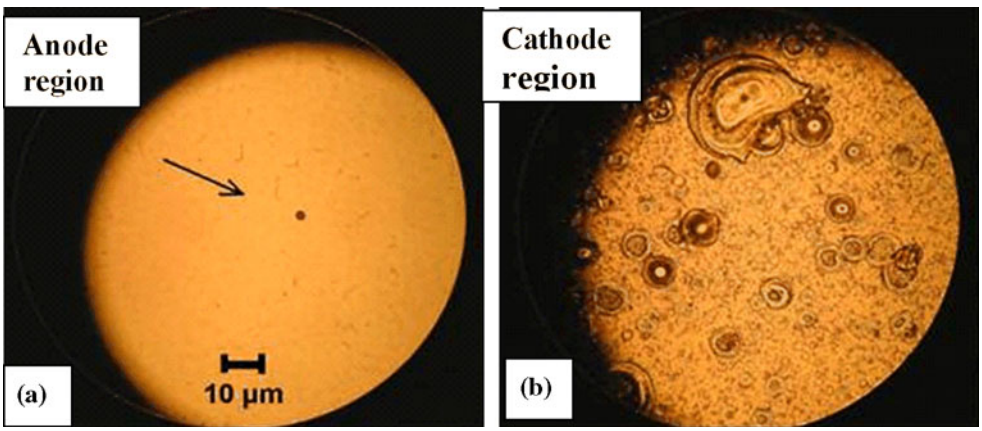

Fig. 3 Al film morphology in the **a** anode and **b** cathode deposited regions

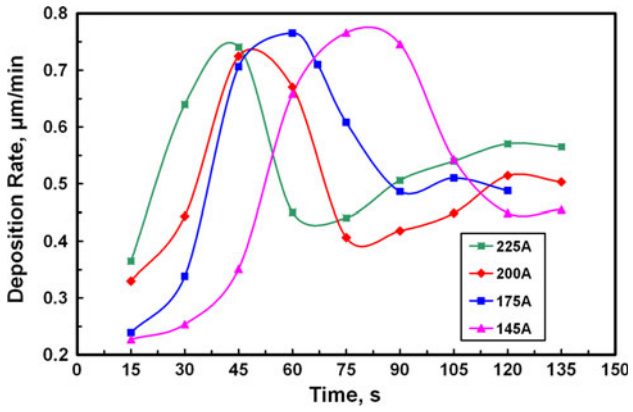

Fig. 4 Time-dependent rate of Al film deposition, $L = 110$ mm, recessed cathode and graphite 30 mm long anode

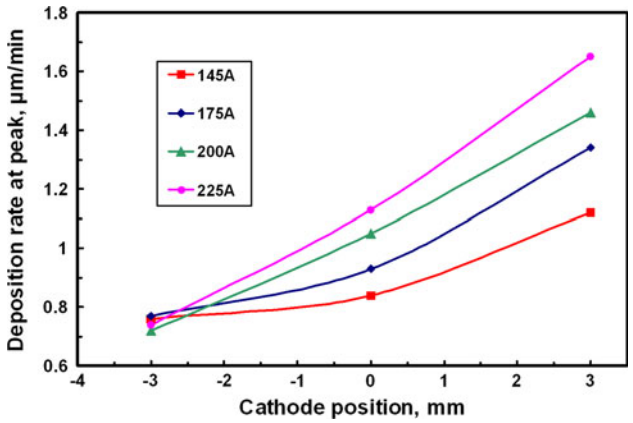

Fig. 5 Peak of deposition rate versus Al-cathode position with respect to the cathode shield edge, $L = 110$ mm, graphite 30 mm long anode

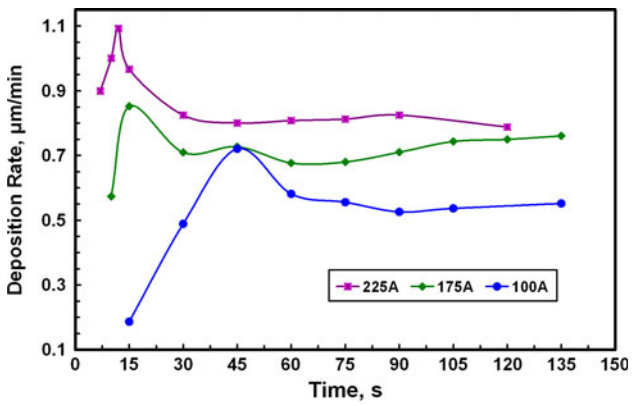

Fig. 6 Al-deposition rate versus time from arc ignition with short graphite 9 mm long anode, $L = 110$ mm (cathode surface was flush mounted with respect to the cathode shield edge)

edge and ~1.7 μm/min when the cathode surface protruded above the shield (for $I = 225$ A and $L = 110$ mm).

Figure 6 shows the Al deposition rate as a function of time obtained using the short graphite anode (9 mm height)

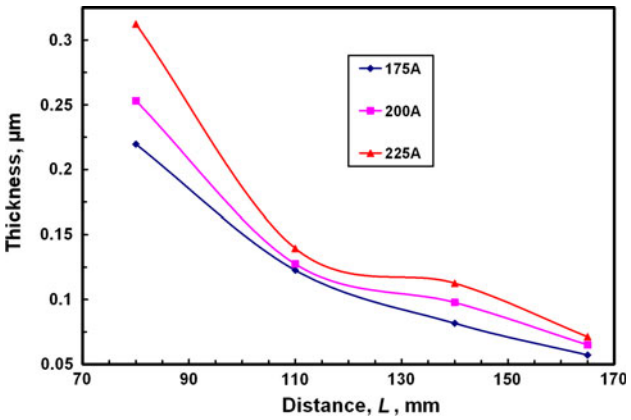

Fig. 7 Maximal Al film thickness as function of distance between the electrode axis and substrate surface; graphite 30 mm long anode (after 90 s arc, recessed cathode)

and the cathode surface flush mounted with respect to the shield edge. It can be seen that the peaks occurred much earlier times than with the 30 mm anode, which the peak width was less, but the peak and steady-state deposition rates were about the same.

The film thickness as a function of distance L between the substrate and the electrode axis is shown in Fig. 7, for 90 s arcs with a recessed cathode. Maximum thickness was obtained at $L = 80$ mm, i.e. closest to the electrodes, ~0.22, 0.25, and 0.30 μm for 175, 200, and 225 A, respectively.

Zinc

The Zn cathode was recessed 3 mm below the end of the cathode shield. Figure 8 presents the measured rate of Zn deposition. In general, the rate increased with currents in all of the arc stages. V_{dep} increased with time from about

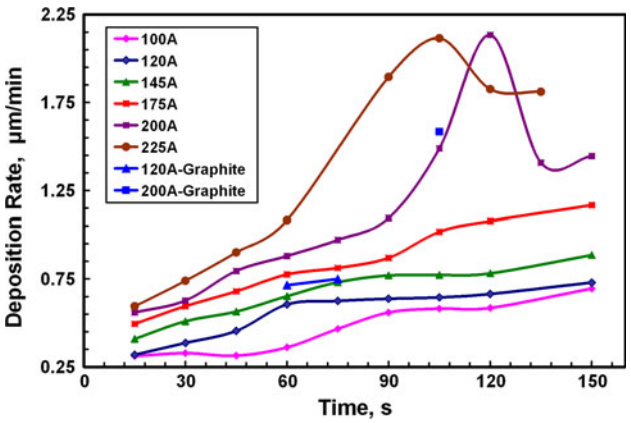

Fig. 8 Zn deposition rate versus time with arc current as a parameter; recessed cathode, 30 mm long Mo anode, $L = 110$ mm. The measured rate of deposition with graphite anode for $I = 120$ and 200 A is presented at three time points

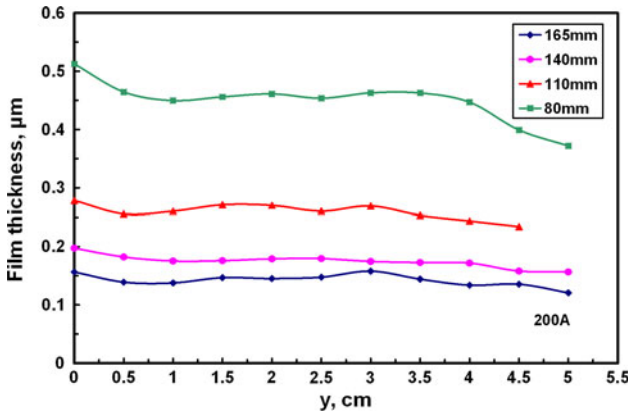

Fig. 9 Dependence of Zn film thickness on distance in direction coaxial with arc axis from A to C boundary in A-region, 200 A, after 90 s arc, 30 mm long Mo anode

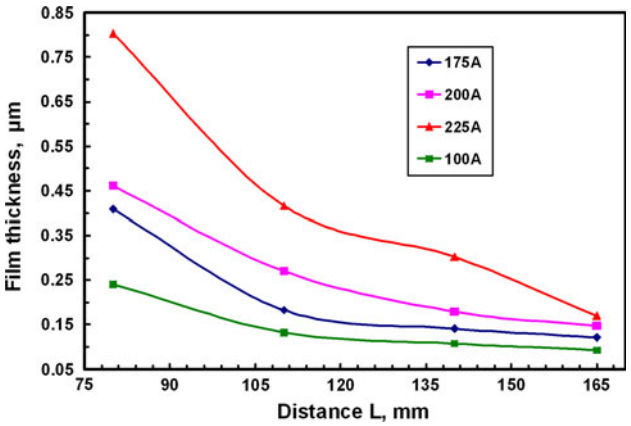

Fig. 11 Dependence of Zn film thickness on distance from arc axis, after 90 s arc, 30 mm long anode

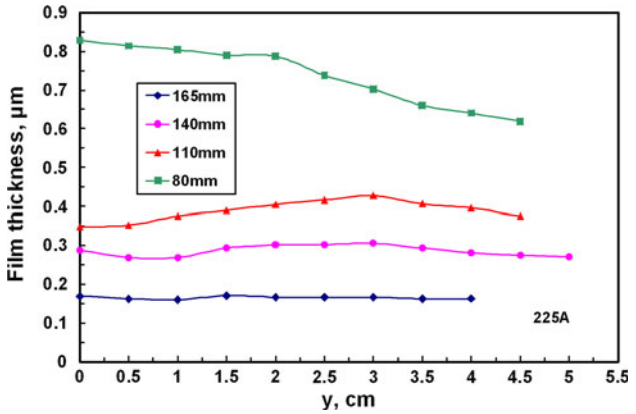

Fig. 10 Dependence of Zn film thickness on distance in direction coaxial with arc axis from A to C boundary in A-region, 225 A, after 90 s arc, anode 30 mm Mo

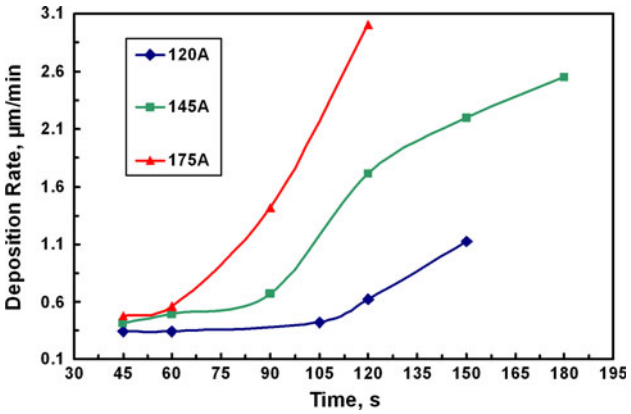

Fig. 12 Dependence of Sn deposition rate on time with current as a parameter (without cathode shield)

0.3 to 0.7 μm/min for 100 A, and from 0.5 to 1.2 μm/min for 175 A during arcing of about 120 s. At higher currents (200 and 225 A), a peak of 2.1 μm/min appeared after ~2 min of arcing. Then, V_{dep} decreased to 1.4 and 1.8 μm/min for 200 and 225 A, respectively. Figures 9 and 10 show the Zn film thickness distribution on the substrate in *y*-direction (see Fig. 1), coaxial with electrode axis in the A-region (from the boundary of A–C regions) for 200 and 225 A, respectively. It can be seen that the film was relatively uniform.

Figure 11 shows that the Zn film thickness decreased with *L*. The maximum thickness, at $L = 80$ mm, was 0.24, 0.4, 0.5, and 0.8 μm for $I = 100$, 175, 200, and 225 A, respectively.

Tin

The rate of Sn deposition is presented in Fig. 12. Initially, V_{dep} was almost constant, but then increased with time after some critical time which decreased with *I*. The arc current affects significantly on V_{dep}. It can be seen that V_{dep} for $I = 175$ A exceed the V_{dep} for 120 A by factor 5 at 2 min of arc duration.

Macroparticle contamination

Al and Zn MP density as function of arc current in the A-region is shown in Fig. 13, for recessed cathodes, $L = 110$ mm, and $t = 60$ s after arc ignition. The Al MP contamination increased almost linearly with current, from about 5 to 32 particles per mm^2 when the current increased from 100 to 225 A. For Zn, the MP density decreased when the current increased from $I = 100$ to 145 A and then increased till $I = 225$ A. The MP density in the A-region of Sn films increased with *I* and exceeded by a several times that in Al films. However, the Sn MP contamination in the A-region was a few orders of magnitude lower than

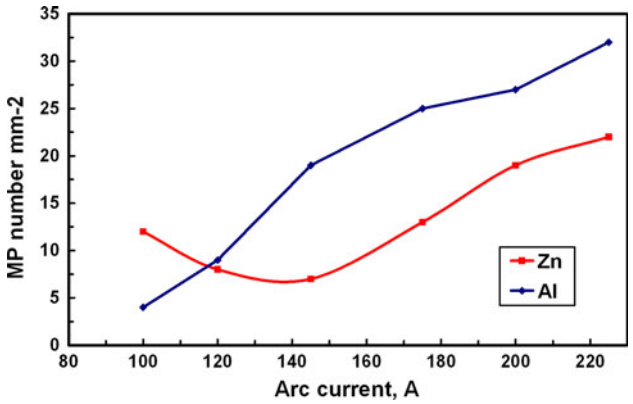

Fig. 13 MP density dependence on arc current in Zn and Al films. 30 mm long anode, $L = 110$ mm, 60 s arc, recessed cathode

in C-region. In the all C-region, the MP density was $\sim 10^3$ mm^{-2} and the MP diameters were in the range of 15–40 μm.

Discussion

The appearance of a peak in the deposition rate versus time graphs can be understood by considering that the cathodes were fabricated from low melting temperature materials. Cathode spots on these materials produced many more MPs than, for example, on Cu cathodes. The MPs accumulated early during the arc on the cold anode surface, and evaporated from the anode during a relatively brief interval when the anode was heated to an appropriate temperature. At the steady-state stage, the MPs previously accumulated at the cold stage significantly disappeared. The deposition rate then declined toward its steady-state value when a balance was achieved between material impingement and evaporation at the hot anode surface. The deposition rate peak was significant for low melting temperature metals such as Al and Zn cathodes, and negligible with Cu, Cr, and Ti cathodes [15, 17]. The peak in the time dependence of deposition rate occurred earlier when using a short anode than a long anode, because the shorter anode was heated faster since it had smaller mass, and reached a higher steady-state temperature due to its radiative heat loss rate was less because of its smaller surface area.

The deposition rate depended on the cathode surface position with respect to the cathode shield. The rate V_{dep} was lower when cathode surface was recessed or flush mounted with respect to the shield comparing to the cathode surface protruded above the shield. This is because the material ejected from the cathode remained on the internal walls of the shield. Therefore, the amount of the cathode material reached the anode surface depends on cathode position and in turn different amount of condensed material was re-evaporated from the anode. As result different intensity of anode plasma plume is radially expanded to the substrate.

The observed MP density for Al, Zn, and Sn cathodes was significantly exceeded this density for cathodes from Cu and Cr [15, 17, 18]. The MP density for Al, Zn was comparable with that for Cu films deposited only when $I < 140$ A. In general, the MP density in the deposited films depends on the relation between the melting point T_m (Al: 660 °C, Sn: 232 °C, Zn: 420 °C) and boiling point T_b (Al: 2447 °C, Sn: 2687 °C, Zn: 907 °C). For the studied above low melting materials, the boiling temperatures of Al and Sn are close to that for Cu (2595 °C) and the generated from the cathodes MP will be evaporated with close rate. However, T_m is lower for Al, Zn and much lower for Sn than for Cu (1083 °C) and therefore the rate of MP generation for Al, Zn, and Sn occurs with larger rates than for Cu. The difference of T_m and T_b for Zn is lower than for Al and therefore the MP density for Zn was observed less than for Al. The difference of T_m and T_b for Sn is larger than for Al and therefore the MP density for Sn was observed larger than for Al.

Conclusion

Thin films of low melting temperature cathode materials (Al, Zn, and Sn) were obtained by HRAVA deposition where the MPs significantly converted to the plasma state at the nonconsumable hot refractory anode surface and in dense anode plasma in the electrode gap. The following main results related to deposition rate and MP contamination can be listed as:

1. The Al and Zn deposition rates initially increased with time to a peak, and then decreased to a steady-state value. The peak occurred due to MP accumulation at the cold anode stage during HRAVA processing and it was earlier when using the shorter anodes.
2. The deposition rate peak changed weakly with the position of an Al-cathode with respect to the shield edge for low current but strongly for high arc current.
3. The HRAVA deposition rate increased with arc current and for different cathode materials was 3, 1.2, and 0.9 μm/min for Sn, Zn, and Al deposition, respectively (at $I = 175$ A).
4. The observed MP density for Al, Zn, and Sn cathodes was significantly exceeded this density for cathodes from Cu and Cr. The MP density for Al, Zn was comparable with that for Cu films deposited only when $I < 140$ A.

References

1. Helmersson U, Lattemann M, Bohlmark J, Ehiasarian AP, Gudmundsson JT (2006) Thin Solid Films 513:1–24
2. Bandyopadhyay SK, Pal AK (1979) J Mater Sci 14:1321. doi:10.1007/BF00549303
3. Park HW, Danyluk S (1991) J Mater Sci 26:23. doi:10.1007/BF00576027
4. Yoshii K, Inoue S, Inami S, Kawabe H (1989) J Mater Sci 24:3096. doi:10.1007/BF01139025
5. Wuhrer R, Yeung WY (2002) J Mater Sci 37:3477. doi:10.1023/A:1016515207089
6. Liu ZW, Yeo SW, Ong CK (2007) J Mater Sci 42:6489. doi:10.1007/s10853-007-1557-2
7. Fan XM, Lian JS, Guo ZX, Zhao L, Jiang Q (2006) J Mater Sci 41:2237. doi:10.1007/s10853-006-7177-4
8. Chandrasekar MS, Shanmugasigamani S, Pushpavanam M (2010) J Mater Sci 45:1160. doi:10.1007/s10853-009-4045-z
9. Boxman RL, Martin P, Sanders D (eds) (1995) Handbook of vacuum arc science and technology. Noyes Publishing, Ridge Park, NJ
10. Beilis II (2001) IEEE Trans Plasma Sci 29:657
11. Martin PJ, Bendavid A (2001) Thin Solid Films 394:1
12. Ehrich H, Hasse B, Mausbach M, Muller KG (1990) J Vac Sci Technol A8(3):2160
13. Kajioka H (1997) J Vac Sci Technol A15:2728
14. Beilis II, Boxman RL, Goldsmith S (2000) Surf Coat Technol 133–134(1–3):91
15. Beilis II, Boxman RL (2009) Surf Coat Technol 204:865
16. Shashurin A, Beilis II, Boxman RL (2009) Plasma Sour Sci Technol 18:045004
17. Beilis II, Snaiderman A, Boxman RL (2008) Surf Coat Technol 203(5–7):501
18. Beilis II, Shashurin A, Arbilly D, Goldsmith S, Boxman RL (2004) Surf Coat Technol 177–178(1–3):233